Pergamon

PII: S0301-9322(96)00064-X

Int. J. Multiphase Flow Vol. 23, No. 1, pp. 131–153, 1997

0301-9322/97 $17.00 + 0.00

A STUDY OF THE PERMEABILITY OF PULP AND PAPER

L. NILSSON and S. STENSTRÖM

Department of Chemical Engineering I, University of Lund, P.O. Box 124, S-221 00 Lund, Sweden

(Received 23 March 1996; in revised form 22 August 1996)

Abstract—A sheet of paper is modelled as a two-dimensional network of cellulose fibres. The fibres are assumed to be either cylindrical or band-shaped. Both well-ordered fibrous structures and fibrous structures in which a random arrangement of fibres is assumed are studied. The equations for creeping flow through such structures are solved, and the calculated permeabilities are compared with measured values. Flow through such paper structures as pulp sheets and handsheets of unbeaten sulphate pulp is found to be adequately described by a structural model that assumes cellulose fibres to be band-shaped when a fibre aspect ratio of 3.5 (well-ordered structure) or 5 (random fibre distribution) is used. These values of the fibre aspect ratio compare favourably with the values used when gas diffusion through the same sheets is modelled. For newsprint sheets the measured permeability is found to be lower than that predicted by the models when physically realistic values for the aspect ratio are taken. It is also found that for all the pulp and paper grades investigated (a total of 19) the measured permeabilities and effective diffusivities correlate with each other. Copyright © 1996 Elsevier Science Ltd.

Key Words: cellulose fibre, computational fluid dynamics, effective diffusivity, Kozeny–Carman theory, permeability, specific surface area

1. INTRODUCTION

For sufficiently slow, steady unidirectional flow through a porous medium the average flow velocity (v) is proportional to the pressure gradient and is inversely proportional to the viscosity (μ) of the flowing fluid. This proportionality, referred to as Darcy's law [1], is the basis of defining the permeability K, a property characteristic of the structure of a porous material. Provided there are no interactions between the fluid and the material, the permeability should remain constant, whatever the physical properties of the flowing fluid are, its value being determined by the size, shape and orientation of the pores

$$v = -\frac{K}{\mu}\frac{\mathrm{d}p}{\mathrm{d}z}. \qquad [1]$$

The capillary flow of liquid water (v_L) is often modelled after Darcy's law [1], the gradient in capillary pressure (p_c) being considered the driving force. The capillary pressure is the pressure difference across the interface between gas and liquid within the pore ($p_c = p_G - p_L$). For capillary flow the product of the permeability to one-phase flow K and the relative permeability K_r serves as the permeability measure

$$v_L = \frac{K \cdot K_r}{\mu}\frac{\partial p_c}{\partial z}. \qquad [2]$$

The relative permeability, which represents the reduction in permeability once the pores of the material are filled with a mixture of two different fluids, is a function of the structure of the material and depends on how well pores of different sizes are connected to each other throughout the material. Couture *et al.* (1994) discuss the question of how the relative permeability can be linked to a measurable quantity: the capillary pressure.

At the Department of Chemical Engineering I in Lund, the physical transport processes involved in industrial paper drying have been studied during recent years. With respect to mass transfer through the material, research within the Department involves an experimental study of the diffusion of water vapour through different pulp and paper grades (Nilsson *et al.* 1993). The diffusion process as measured was later modelled as gas-diffusion around the band-shaped cellulose

fibres (Nilsson and Stenström 1995a, b). However, mass transfer within the drying web takes place not only through the diffusion of water vapour but also through the capillary flow of liquid water. Accordingly, one way of obtaining further information on the drying process is to measure moisture gradients in the drying material (Nilsson *et al.* 1996a). Research on mass transfer through sheets of pulp and paper aims at obtaining an understanding of the mass transfer processes involved in transporting liquid water and water vapour from the interior of the sheet to its surface during the drying process.

Convective drying of a porous material occurs in two periods; the constant rate period and the falling rate period. During the constant rate period the drying material behaves as a wet surface, and the drying rate is constant and independent of the moisture content of the material. The drying rate is solely determined by an energy balance between the heat supplied to the material and the water evaporated from the material. The constant rate period prevails as long as capillary suction of liquid water from the larger pores in the interior of the paper sheet to the surface keeps the surface sufficiently wet (Schlünder 1988). In the falling rate period the mechanisms determining the total drying rate are more complex. When drying a hygroscopic material, the equilibrium vapour pressure at low moisture contents decreases below that of pure water. Another reason is that capillary flow of water does not equalise the moisture content throughout the material. A region of lower moisture content then arises close to the surface where drying occurs. Measured curves for the drying of paper show that the drying rate starts to decrease at total moisture contents of between 62% and 78% (Göttsching and Rhodius 1978). A decreasing drying rate at such high levels of total moisture content cannot be explained by hygroscopic effects alone. Evidently, capillary flow of liquid water is not sufficient to distribute the water evenly throughout the material.

Other transport processes that are connected with pulp and paper processing, and in which the permeability of the material is central to an understanding of the process taking place, involve the migration of water into the base paper during the coating of paper, moisture uptake in corrugated media kept in storage-rooms, and the delamination of paper during impulse drying (Persson 1994).

The present study investigates the permeability of pulp and paper both theoretically and experimentally. It is assumed that macroscopic flow occurs in the direction of the sheet thickness only and that all fibres are perpendicular to the macroscopic direction of flow. The permeability is calculated both for structures with a regular arrangement of fibres and for those in which a random fibre arrangement is assumed. A sheet of paper is built up of a large number of cellulose fibres, each approximately 20–40 μm in width and 2–5 mm in length. The structure of the sheet is stabilised by the hydrogen bonds between the cellulose fibres. The fibre orientation is predominantly random in the plane of the sheet, with certain alignment of the fibres in the machine direction.

The theoretical models describing flow through such fibrous structures will be compared with experimental data for air flow through pulp and paper. How the permeabilities measured correlate with other material properties measured for the samples, including the volume fraction of fibres, the effective diffusivity, the specific surface area and the fibre orientation ratio are discussed.

2. PREVIOUS WORK

Whereas the flow in porous media is described macroscopically by Darcy's law [1], the processes taking place on a microscopic scale are described by the Navier–Stokes equations. At sufficiently low Reynolds numbers (approximately $\mathrm{Re} < 0.1$), the convective terms in the Navier–Stokes equations can be ignored, the remaining set of differential equations being termed the Stokes equations or the equations for creeping flow. It is at such low Reynolds numbers that Darcy's law [1] is valid with a constant permeability.

Previously, solutions to the differential equations describing flow in porous media were only available for some few simple geometries. In much of the work on flow and diffusion in porous media, the pore structure has thus been modelled as a bundle of conduits penetrating the whole thickness of the material, since the flow through such conduits can be described by a generalisation of the Hagen–Poiseuille equation, a shape factor k_0 taking account of the non-circularity of the conduit. Assuming that all conduits are equal in length, cross-sectional shape and size, the relation

between the permeability K and the volume fraction of fibres ϕ is described by the well-known Kozeny–Carman equation (Carman 1937; Kozeny 1927):

$$K = \frac{(1-\phi)^3}{k_0 \tau^2 \phi^2 \tilde{A}_s^2} \quad [3]$$

where τ is the tortuosity, defined as the ratio of the real conduit length to the length of a hypothetical straight conduit. $\tilde{A}_s$ is the specific surface area of the material, and originally suggested values for the shape factor k_0 range from 2 (circular cross-section) to 3 (rectangular slit). The disadvantages of [3] is that measurements of the specific surface area of the sample cannot alone be used for predicting permeability, since for most porous materials knowledge of the tortuosity is lacking.

Fluid flow in fibrous porous media containing cylindrical fibres was first dealt with by Happel (1959) in a cell model theory. This study involved dividing the system into a number of equidimensional subsystems and calculating the fluid flow in any given subsystem by solving the Stokes equations analytically. The flow within a subsystem is taken then to be representative of the flow through the macroscopic material as a whole. The resulting equation relating permeability to the volume fraction of fibres when the cylinders are normal to the main flow direction is:

$$\frac{K}{D_h^2} = \frac{1}{32\phi}\left(-\ln(\phi) - \frac{1-\phi^2}{1+\phi^2}\right). \quad [4]$$

D_h representing the hydraulic fibre diameter, which for cylindrical fibres equals the diameter. Happel's free surface model has previously been applied to pulp and paper technology when modelling mechanical dewatering of pulp (Jönsson and Jönsson 1992a, b).

Later theoretical studies provided numerical solutions to the Stokes equations for various ordered arrangements of cylindrical fibres, including both hexagonal and square arrays. Such studies involved calculating the permeability perpendicular to (Sangani and Acrivos 1982) as well as parallel to (Drummond and Tahir 1984) the fibre direction.

Theoretical as well as experimental work concerning creeping fluid flow in fibrous porous media consisting of cylindrical fibres was reviewed by Jackson and James (1986). Measured permeabilities are generally higher than those calculated for ordered fibre arrays. This can be explained on the basis of the randomness within the real structures, a combination of different pore sizes leading to higher permeabilities than in structures with pores of equal size such as those used for theoretical modelling.

Solutions to the Stokes equations for creeping flow through clusters of elliptical cylinders were obtained by Epstein and Masliyah (1972) and by Brown (1975). In both these studies it was found that for flow past elliptical cylinders with their major axes normal to the main flow direction the permeability decreases with increasing flatness of the fibres.

Permeability measurements made for beds of flattened fibres with well-defined aspect ratios, together with permeability measurements made for beds of wood pulp fibres at various degrees of fibre collapse, led Bliesner (1964) to the conclusion that results obtained in studies of cylindrical fibres could not be applied to collapsed wood pulp fibres. Labrecque (1968) measured the permeability for beds of flattened fibres with well defined shapes. In the range of aspect ratios up to 3:1 he found very little effect of the fibre cross-sectional shape on fluid flow resistance. Between aspect ratios of 3:1 and 4.69:1 (the latter being the highest fibre aspect ratio investigated) the permeability was found to decrease significantly with increasing aspect ratio.

Extensive experimental studies of the permeability of paper to water have been performed (Lindsay and Brady 1993a, b). The experimental equipment used in these studies allowed both the transverse (thickness direction) permeability and the lateral (in-plane) permeability of paper to be evaluated. Paper was found to be a highly anisotropic material, since the quotient of the lateral to the transverse permeability was in the range of 2–40. Further work involved studying the effect of water removal on the transverse permeability of subsequently resaturated sheets. Partial water removal to 40% solids followed by resaturation resulted in an increase in permeability by a factor of 10 as compared with sheets that were always kept saturated (10–20% solids). Complete water removal at 108° followed by resaturation resulted in an increase in permeability by a factor of 100.

These changes in permeability reflect structural changes occurring during the drying process, including the rearrangement of fines by capillary forces and partial or total fibre hornification. Fibre hornification involves the permanent closing of many of the small pores in the cellulose fibre by surface forces, reducing the swelling capacity of the fibre. As a consequence, when the sheet is rewetted, less water can be associated with the cellulose. For a rewetted sheet and a newly formed sheet of the same total porosity, the volume of the open space between the fibres is greater in the rewetted sheet, whereas the porosity in the fibre wall is greater in the newly formed sheet.

Computational fluid dynamics was used to model the laminar flow of fluids through a fibre mat with a porosity gradient (Sampson and Bridle 1995). The structure of the fibre mat was described firstly as representing five serially connected porous media of differing porosity, the permeability of each medium being obtained from the Kozeny–Carman equation [3] on the assumption that $k_0\tau^2 = 5.5$. Secondly, the flow process of the fibre dimension was investigated, the structure being described as consisting of five layers of fibres of differing degrees of fibre collapse and porosity. The results of both these computations show the major resistance to flow to be that in the least porous layer.

Wang (1996) provided rigorous, analytical solutions to the Stokes equations for a well-ordered array of rectangular fibres, relating the permeability of such an array to three geometric ratios characterising the structure. It was demonstrated how the analytically calculated permeabilities are reduced to expressions based on the Kozeny–Carman equation provided that the channel length in the array is at least five times the channel width. Regarding the permeability of structures consisting of flattened fibres, it was found that the permeability of flow facing the shorter side of the fibre cross-section is much higher than for flow facing the longer side.

3. THEORETICAL MODELS

In every case discussed below, solutions to the Navier–Stokes equations at steady-state for a two-dimensional system are sought, the influence of gravity on the flow process studied being neglected:

$$\rho\left(v_x\frac{\partial v_x}{\partial x} + v_y\frac{\partial v_x}{\partial y}\right) = -\frac{\partial p}{\partial x} + \mu\left(\frac{\partial^2 v_x}{\partial x^2} + \frac{\partial^2 v_x}{\partial y^2}\right)$$

$$\rho\left(v_x\frac{\partial v_y}{\partial x} + v_y\frac{\partial v_y}{\partial y}\right) = -\frac{\partial p}{\partial y} + \mu\left(\frac{\partial^2 v_y}{\partial x^2} + \frac{\partial^2 v_y}{\partial y^2}\right). \quad [5]$$

For transport in porous media, the Reynolds number is often below 10^{-1}, allowing the convective terms on the left-hand side in [5] to be ignored. For this specific study, this assumption is validated in the appendix. As a consequence of this assumption, the following set of differential equations [6], often termed the Stokes equations or the equations for creeping flow, are assumed to describe the flow process studied:

$$0 = -\frac{\partial p}{\partial x} + \mu\left(\frac{\partial^2 v_x}{\partial x^2} + \frac{\partial^2 v_x}{\partial y^2}\right)$$

$$0 = -\frac{\partial p}{\partial y} + \mu\left(\frac{\partial^2 v_y}{\partial x^2} + \frac{\partial^2 v_y}{\partial y^2}\right). \quad [6]$$

For incompressible steady flow in two dimensions, the equation for continuity takes the form of [7] below:

$$\frac{\partial v_x}{\partial x} + \frac{\partial v_y}{\partial y} = 0. \quad [7]$$

For solving the differential equations above for the different geometries and the different combinations of boundary conditions listed below, a fluid dynamics analysis package FIDAP V7.06 was employed.

3.1. Cylindrical fibres

3.1.1. Free surface models. Free-surface models were first introduced by Happel (1959), who solved the equations for creeping flow [6] around one solid cylindrical fibre of radius b surrounded by an envelope of fluid of radius R, as shown in figure 1, the following boundary conditions being assumed:

$$v_x|_{r=b} = 0$$

$$v_y|_{r=b} = 1 \qquad [8]$$

$$v_r|_{r=R} = 0 \qquad [9]$$

$$\tau_{r\theta}|_{r=R} = 0. \qquad [10]$$

The boundary condition denoted in [8] involves assuming that the solid cylinder moves through the fluid envelope along the y-axis at a constant velocity, its being assumed in the model that the fibre moves whereas no net motion of the fluid occurs. The boundary condition in [9] states that there is no fluid flow out of the envelope. Finally, [10] states that there is no shear ($\tau_{r\theta}$) at the outer boundary.

The drag force on the fibre can be obtained through integrating the traction along the surface of the fibre. However, in the present numerical study the energy equation [11] was solved along with the Stokes equations [6] so as to obtain the temperature distribution within the fluid envelope

$$\rho C_p\left(v_x\frac{\partial T}{\partial x} + v_y\frac{\partial T}{\partial y}\right) = k\left(\frac{\partial^2 T}{\partial x^2} + \frac{\partial^2 T}{\partial y^2}\right) + 2\mu\left(\left(\frac{\partial v_x}{\partial x}\right)^2 + \left(\frac{\partial v_y}{\partial y}\right)^2\right) + \mu\left(\frac{\partial v_x}{\partial y} + \frac{\partial v_y}{\partial x}\right)^2. \qquad [11]$$

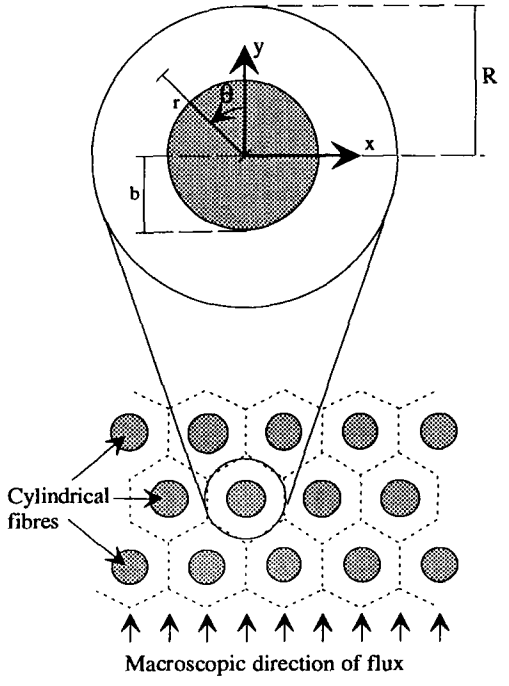

Figure 1. The structure of the material containing cylindrical fibres and the definition of the cell used in the free-surface model.

The boundary conditions for the energy equation involve assuming there to be no heat transport out of the outer boundary of the fluid envelope [12] and the surface temperature of the fibre to be constant [13]:

$$\left.\frac{\partial T}{\partial r}\right|_{r=R} = 0 \qquad [12]$$

$$T|_{r=b} = 20. \qquad [13]$$

From the numerical solution, the amount of energy converted from mechanical energy into heat (P) can then be obtained as the amount of heat conducted into the solid cylinder. By relating the energy loss to the pressure drop in terms of a balance of forces [14], the permeability of the structure can be calculated from Darcy's law [1]

$$\frac{P}{\pi R^2 v_y|_{r=b}} = -\frac{\mathrm{d}p}{\mathrm{d}z}. \qquad [14]$$

As evident in figure 3, the numerically calculated permeabilities FIDAP provides for the free-surface model agree very well indeed with those calculated using [4].

3.1.2. Hexagonally arranged structure. The unit cell for a hexagonal array of cylinders is shown in figure 2. The boundary conditions employed are as follows:

$$v_x|_{0<x<a,y=0} = v_x|_{b<x<a+b,y=\sqrt{3}(a+b)} = v_x|_{x=0,0<y<\sqrt{3}a+(\sqrt{3}-1)b} = v_x|_{x=a+b,b<y<\sqrt{3}(a+b)} = 0 \qquad [15]$$

$$(v_x, v_y)|_{a<x<a+b,y=\sqrt{b^2-(x-(a+b))^2}} = (v_x, v_y)|_{0<x<b,y=\sqrt{3}(a+b)-\sqrt{b^2-x^2}} = (0,0) \qquad [16]$$

$$\frac{\displaystyle\int_b^{a+b}\left(-p+2\mu\frac{\partial v_y}{\partial y}\right)\mathrm{d}x\Big|_{y=\sqrt{3}(a+b)}}{a} - \frac{\displaystyle\int_0^{a}\left(-p+2\mu\frac{\partial v_y}{\partial y}\right)\mathrm{d}x\Big|_{y=0}}{a} = 1. \qquad [17]$$

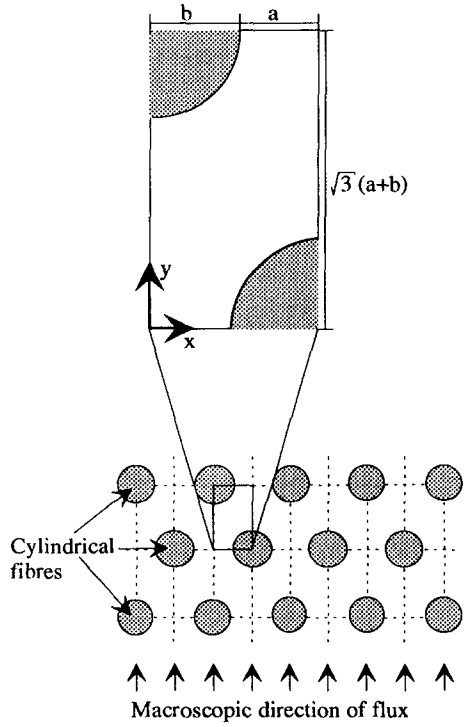

Figure 2. The structure of the material containing cylindrical fibres and the definition of the cell used for material consisting of hexagonally arranged cylinders.

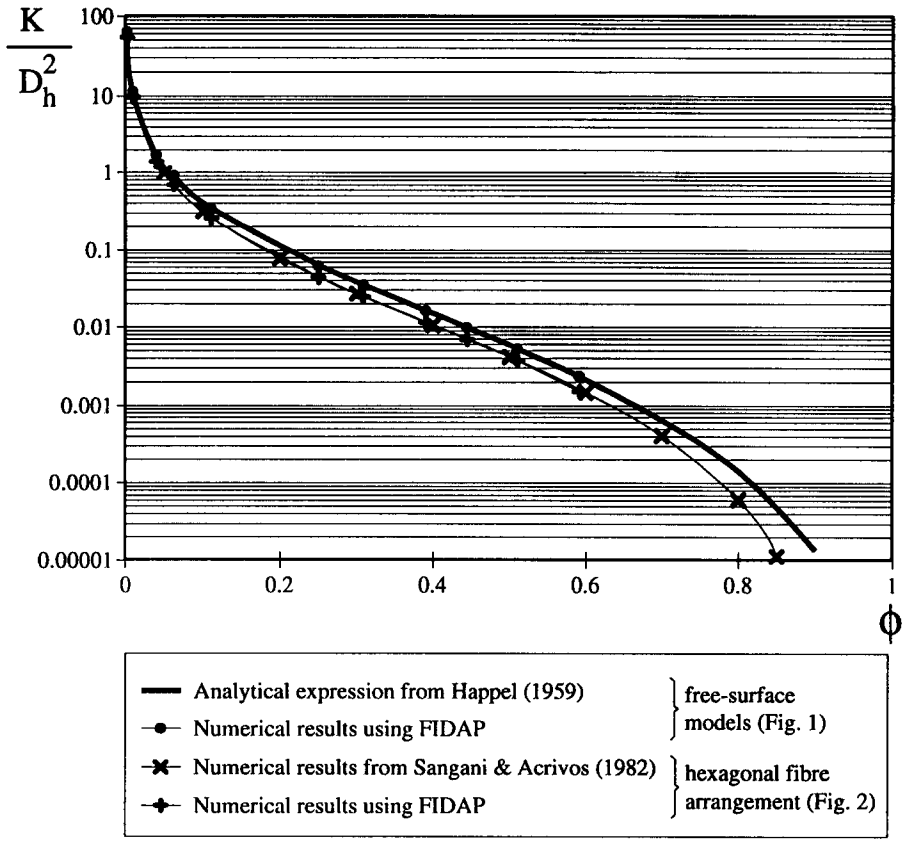

Figure 3. Calculated permeabilities for a material containing cylindrical fibres. Comparison of the permeabilities calculated using FIDAP with those based on the analytical expression [4] for the free-surface model. Comparison of the permeabilities calculated using FIDAP with the numerical calculations reported by Sangani and Acrivos (1982) for hexagonally arranged fibres.

Equation [15] states that on grounds of symmetry there is no x-direction velocity at any of the symmetry lines. Equation [16] expresses the no-slip condition at the cylinder surfaces. Equation [17], which describes a boundary condition for normal stress at the inlet and the outlet, states that the average pressure drop across unit cell equals 1 Pa. It should be emphasised that the latter equation does not imply a constant pressure along the entrance and exit boundaries of the unit cell. Instead, the pressure varies along these two boundaries, being lowest at the surface of a cylindrical fibre. The volumetric rate of flow across the inlet and the outlet boundaries of the unit cell is calculated directly. Since the pressure drop and the dimensions of the unit cell are known, the permeability can be obtained directly from Darcy's law [1].

As evident in figure 3, agreement between the present numerical results and previous numerical results (Sangani and Acrivos 1982) is more than satisfactory.

3.1.3. Comparison between the different models. The data in figure 3 allow a comparison between the two different models for treating fluid flow around cylindrical fibres. There is fair agreement between the permeabilities calculated from these two different models, and only at high volume fractions of fibres (approximately $\phi > 0.8$) will the permeability calculated from the hexagonal fibre array decrease more rapidly with increasing ϕ than that calculated using the free-surface model. This is because $\phi \approx 0.907$ is the maximum ϕ-value allowed in a hexagonal fibre arrangement, whereas the equations for the free-surface model can be solved for all volume fractions of fibres up to $\phi = 1.0$, even though it is not possible to pack cylindrical fibres as close together as that.

3.2. Band-shaped fibres

3.2.1. Free-surface models. The geometry involving band-shaped fibres of width b and height h is shown in figure 4. The boundary conditions are analogous to those employed for cylindrical fibres. They include the assumption of a constant y-direction velocity at the fibre boundary

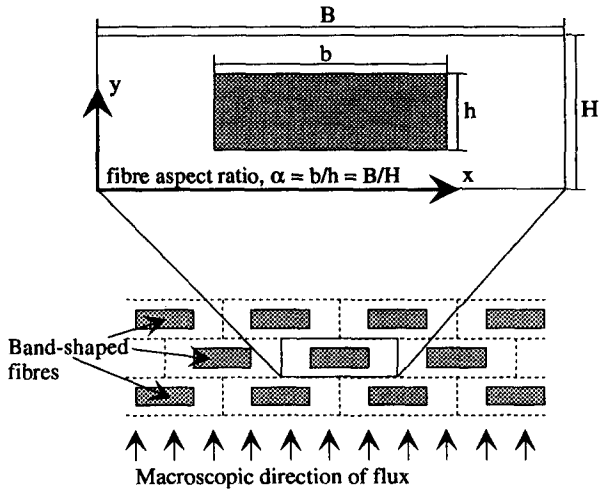

Figure 4. The structure of the material containing band-shaped fibres and the definition of the cell used in the free-surface model.

(analogous to [8]), that of there being no velocity at the outer boundary of the fluid envelope (analogous to [9]) and finally of there being no shear at the outer boundary of the fluid envelope (analogous to [10]).

The permeability of the structure can be calculated by solving the combination of the Stokes equations [6] and the energy equation [11] in a manner analogous to that described above, viz. through calculating heat loss, a balance of forces on the fibre and use of Darcy's law [1].

In figure 5 the permeabilities calculated for different values of the fibre aspect ratio α are shown. With an increase in the aspect ratio, the permeability decreases.

3.2.2. Ordered arrangement of band-shaped fibres. For such a well-ordered arrangement of band-shaped fibres as that shown in figure 6, the permeability can be calculated by solving the Stokes equations [6] in combination with boundary conditions analogous to those employed for hexagonally arranged cylindrical fibres. These boundary conditions include assuming for reasons of symmetry that there is no x-direction velocity at the four boundaries of the unit cell (analogous

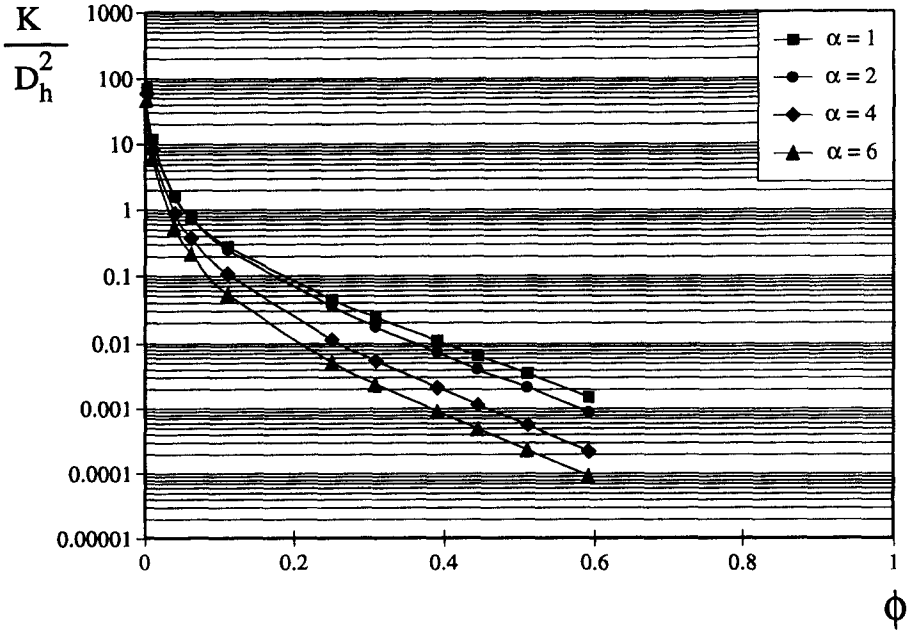

Figure 5. The permeabilities for $\alpha = 1$, 2, 4 and 6 using FIDAP.

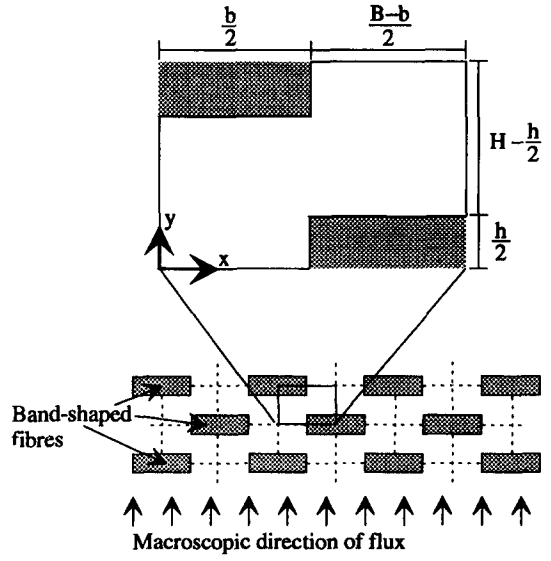

Figure 6. The structure of the material containing band-shaped fibres and the definition of the cell used when treating the material as a well-ordered structure.

to [15]), that the velocity at the fibre surfaces is zero (analogous to [16]) and finally that the pressure drop over the unit cell equals 1 Pa (analogous to [17]). Once the Stokes' equations [6] have been solved, the permeability can be obtained directly from Darcy's law [1].

In figure 7 the permeabilities calculated are shown for different values of the fibre aspect ratio. For a low volume fraction of fibres ($\phi < 0.10$), the permeability hardly seems to depend on the aspect ratio. For higher volume fractions of fibres, the permeability decreases with increasing fibre aspect ratio.

3.2.3. Comparison between the different models. Figure 8 compares the two different models for treating fluid flow around band-shaped fibres, two different values for the aspect ratio being employed, $\alpha = 1$ and 6. For quadratic fibres ($\alpha = 1$), the agreement between the permeabilities calculated by the two different models is very good over the whole range of volume fractions of

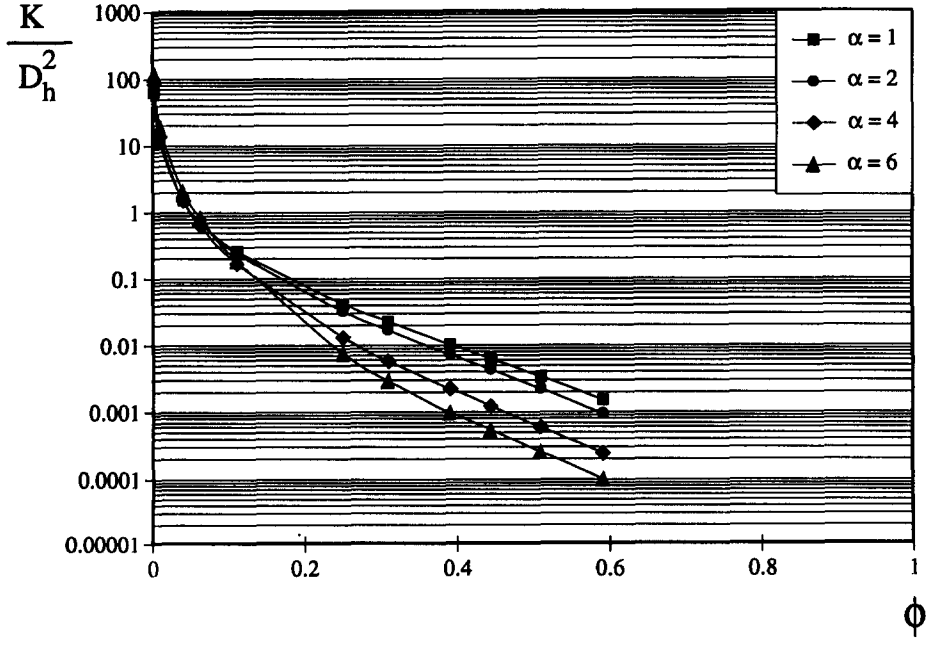

Figure 7. The permeabilities calculated for $\alpha = 1$, 2, 4 and 6 using FIDAP.

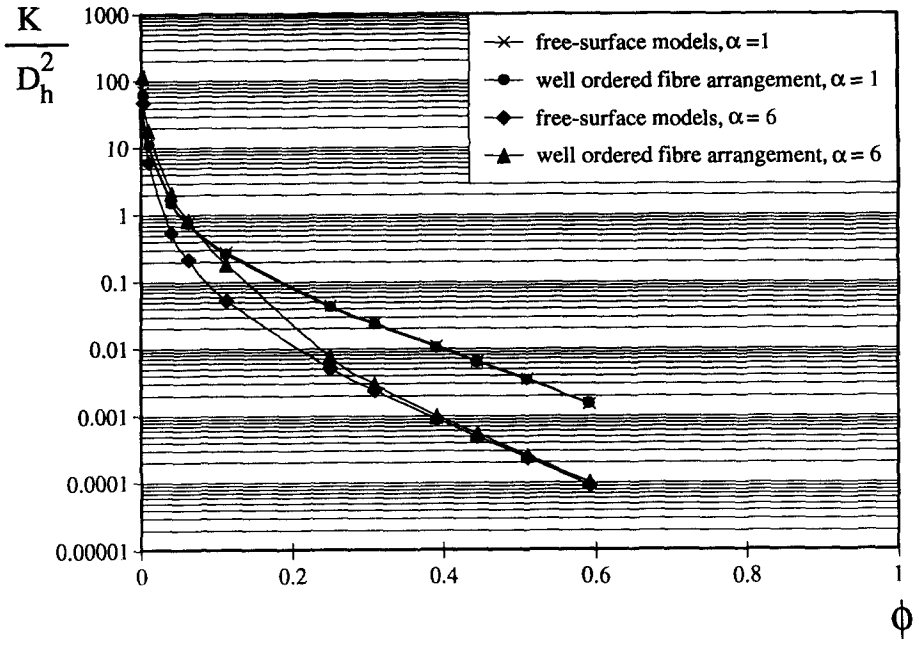

Figure 8. Permeabilities for a medium consisting of band-shaped fibres. Comparison for $\alpha = 1$ and 6 of permeabilities obtained for a free-surface model and for a model assuming a well-ordered structure.

fibres, just as it was for cylindrical fibres. For the band-shaped fibres ($\alpha = 6$), the agreement is quite poor for $\phi < 0.20$, the free-surface models predicting much lower permeabilities there than those calculated from the ordered fibre arrangement. For $\phi > 0.30$ the agreement is again very good. The reason for agreement between the two models being poor at a volume fraction of fibres of $\phi < 0.20$ is the difference between the two models in the flow patterns predicted. For the ordered fibre arrangement, flow at low volume fractions of fibres occurs mainly in the pores to the left and the right of the fibres, whereas the velocities in the pore to spaces above and below the fibres are very low. For the free-surface model, on the other hand, the boundary conditions imposed state that the relative velocity of the fibre and the surrounding fluid is constant. Thus, for that model, there is considerable fluid motion in the x-direction, also in the narrow passages above and below the fibre at all different values of ϕ.

3.3. Structures involving a random arrangement of fibres

In order to estimate the effect of random fibre distribution on the permeabilities calculated, paper cross-sections consisting of band-shaped cellulose fibres were computer-generated. Structures of this type are generated by randomly placing a number of fibres in the paper cross-section until a certain porosity is reached. If the new fibre is allocated a position where it interferes with a fibre already present in the cross-section, it is taken away and placed somewhere else. This algorithm guarantees that there is no contact between the fibres in the cross-section, although the pores between fibres can of course be infinitely narrow. When generating structures, it was further assumed that all the fibres have equal size and equal aspect ratios. Such a computer-generated paper cross-section, one with an aspect ratio of $\alpha = 5$ and a volume fraction of fibres of $\phi = 0.50$, is shown at the centre of figure 9.

Twenty random structures with a volume fraction of fibres of $\phi = 0.30$, 20 with $\phi = 0.40$ and 20 with $\phi = 0.50$ were generated for aspect ratios of $\alpha = 2$, 5 and 8, resulting in a total of 180 random structures. These combinations of α and ϕ were chosen so as to be realistic for the paper material. The total volume fraction of fibres of a commercial paper grade seldom exceeds 0.45 (see table 2). When generating the random structures, the size of each fibre cross section was taken as a first crude assumption to be 5×25 μm, so that the hydraulic diameter of a fibre was thus $D_h \approx 8.33$ μm. The size of the entire structure shown in figure 9 is 28.28×141.42 μm.

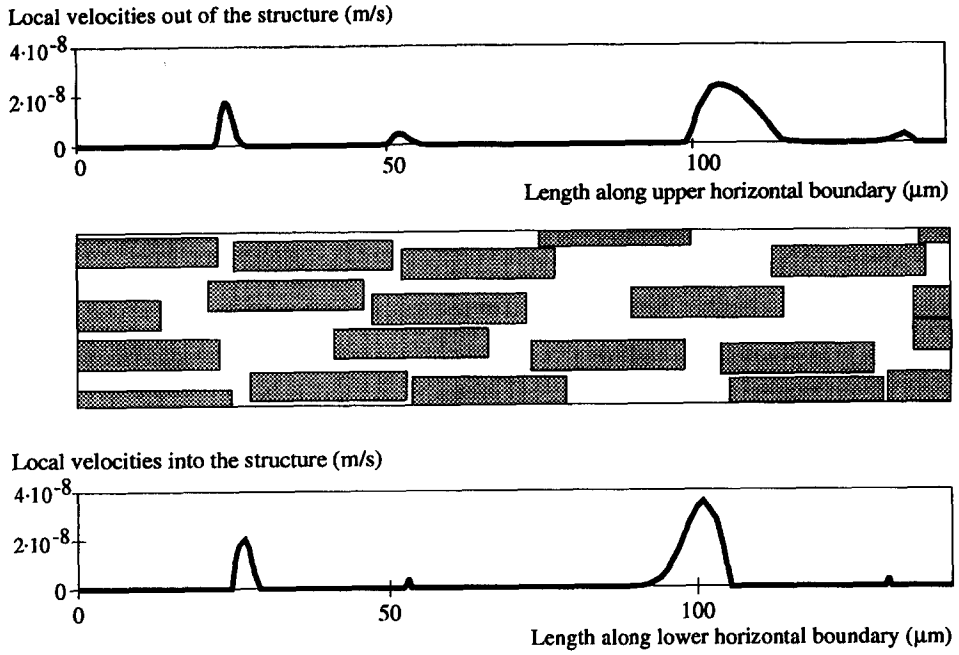

Figure 9. Random structure consisting of band-shaped fibres with $\alpha = 5$. Also shown is the flux into and out of the structure as a function of position along the boundaries.

Once the structure has been generated, the permeability can be calculated by solving the Stokes equations [6] for the structure. The boundary conditions employed are those below:

$$(v_x, v_y)|_{\text{fibre surfaces}} = (0, 0) \qquad [18]$$

$$v_x|_{\text{vertical boundaries}} = 0 \qquad [19]$$

$$\frac{\displaystyle\int_{\text{upper horizontal boundary}} \left(-p + 2\mu \frac{\partial v_y}{\partial y}\right) \mathrm{d}x}{\text{length of upper horizontal boundary}} - \frac{\displaystyle\int_{\text{lower horizontal boundary}} \left(-p + 2\mu \frac{\partial v_y}{\partial y}\right) \mathrm{d}x}{\text{length of upper horizontal boundary}} = 1. \qquad [20]$$

In [18] it is assumed that the no-slip condition holds for all the fibre surfaces, and in [19] that there is no flow across the two vertical boundaries. Equation [20] is a boundary condition for the normal stress at the inlet horizontal boundary and the outlet horizontal boundary, stating that the pressure drop over the structure equals 1 Pa.

For that specific random structure appearing in the middle of figure 9 it is indicated how the local flow velocities into the structure and out of the structure vary along the lower horizontal boundary and the upper horizontal boundary, respectively. According to the numerical solution to the problem, the pressure varies less than 0.01 Pa along the boundaries. Evidently viscous forces are negligible compared with pressure forces. The boundary condition given in [20] is reduced with acceptable accuracy to simply stating constant pressures at the two horizontal boundaries, as is shown in [21]:

$$p|_{\text{upper horizontal boundary}} = p_{\text{ref}}$$

$$p|_{\text{lower horizontal boundary}} = p_{\text{ref}} + 1. \qquad [21]$$

The average velocity v through the structure can be calculated by integrating the local velocities shown in the graphs and dividing by the length of the horizontal boundary. The average flow velocity thus obtained is $v = 2.31 \times 10^{-9}$ m/s. Since the length of the structure ($L = 28.28$ μm) and the pressure difference between the two horizontal boundaries ($\Delta P = 1$ Pa) are known and the viscosity was set to be $\mu = 1$ Pas, one can determine directly from Darcy's law [1] that $K = 6.54 \times 10^{-14}$ m^2 for that specific structure and that $K/D_h^2 = 9.4 \times 10^{-4}$.

Table 1. The average dimensionless permeabilities for structures with a random fibre arrangement as compared with those calculated using free-surface models or assuming a highly ordered fibre arrangement

Fibre aspect ratio α	Volume fraction of fibres ϕ_e	K/D_h^2			
		Random fibre arrangment		Free-surface models	Ordered fibre arrangement
		Average value	Standard deviation		
2	0.30	0.0244	0.0090	0.0199	0.0190
	0.40	0.0100	0.0090	0.00667	0.00674
	0.50	0.00335	0.00270	0.00239	0.00253
5	0.30	0.0195	0.0101	0.00411	0.00475
	0.40	0.00633	0.00400	0.00124	0.00133
	0.50	0.00109	0.00061	0.000401	0.000433
8	0.30	0.0142	0.0086	0.00113	0.00177
	0.40	0.00282	0.00190	0.000540	0.000670
	0.50	0.000500	0.000358	0.000126	0.000130

In table 1 the average of the permeabilities is given for each combination of α and ϕ, together with the standard deviation and the corresponding values of the permeabilities as calculated from the free-surface models or from the assumption of a well-ordered fibre arrangement. Introducing a random distribution of fibres evidently increases the permeability as compared with those structures for which a uniform fibre distribution is assumed.

4. EXPERIMENTAL

In the experimental part of this study the basis weight, the thickness, the quotient of the effective water vapour diffusivity to the water vapour diffusivity in air, the permeability, the specific surface area and the fibre orientation ratio of 21 different pulp or paper samples were measured (see table 2).

The pulp or paper thickness was measured using a micrometer with spherical platens (Fellers *et al.* 1986). This method was preferred since it provides an average thickness, which should be suitable for comparison with model predictions regarding transport through the paper structure.

The effective water vapour diffusivity of the samples was measured in a diffusion cell at 60°C (Nilsson *et al.* 1993).

The permeability of the samples was measured by the Gurley method (SCAN-P 19:78). With this method, air is allowed to penetrate the sample under a standardised pressure difference (1210 Pa). The time needed for 10^{-4} m^3 of air to pass the sample is measured when the sample area available for penetration is 6.47×10^{-4} m^2. The coated LWC-sheets have a very high resistance to air flow, beyond the range suitable for this method, and for those sheets it was not possible to obtain reproducible results.

The specific surface areas of the pulp and paper samples were measured by the one-point BET-method, using nitrogen as the adsorbent (Brunauer *et al.* 1938). In table 2 $\hat{A}_s$ denotes the surface area related to the mass of the sample, whereas $\tilde{A}_s$ denotes the surface area related to the dry substance volume of the sample. The measurements were performed on a FLOWSORB 2300. The gas consisted of 30% N_2 and 70% He. In some cases the BET-method has been used for characterising different paper grades (Lindström and Söderberg 1986). It has been observed furthermore that the adsorption isotherms on cellulose follow the predictions of the BET model over its usual range of applicability (Mohlin and Gray 1974).

The tensile stiffness index (TSI) of a paper sheet is highest in that direction where most fibres are oriented (the machine direction) and lowest in that direction where the fewest fibres are oriented (the cross direction). Also, the ultrasonic speed is considerably higher in the fibre direction than in the direction perpendicular to the fibres. This fact is used to evaluate the tensile stiffness index and thereby the fibre direction in the paper sheet by measuring the ultrasonic velocity in several directions in the plane of the sheet. The directionality is reported here as the quotient of the maximum to the minimum value of the tensile stiffness index (TSI_{max}/TSI_{min}). That quotient relates the number of fibres oriented in the most frequently occurring direction to the number of fibres

Table 2. Some measured physical properties of the pulp/paper qualities investigated

Paper grade		Basis weight (g/m^2)	Volume fraction Thickness (μm)	Reduction of the of fibres ϕ_{tot}	Permeability diffusivity D_e/D_g	Specific surface area $K \times 10^{15}$ (m^2)	Specific surface area $\hat{A}^s$ (m^2/g)	Fibre orientation $\tilde{\tilde{A}}_3 \times 10^{-6}$ (m^2/m^3)	$\frac{TSI_{max}}{TSI_{min}}$
Filter paper		129	285	0.281	0.22	1100	1.1	1.7	1.7
Sack paper		79	91	0.539	0.013	10	0.52	0.84	1.6
Liner		148	201	0.457	0.013	8.5	0.89	1.4	2.4
		148	201	0.457	0.013	7.1	1.0	1.6	2.6
		294	411	0.444	0.021	23	0.90	1.5	2.4
		294	411	0.444	0.022	17	0.92	1.5	2.8
LWC-paper	Before coating and calendering	41	58	0.439	0.010	1.7	0.98	1.6	5.5
	After coating, before calendering	61	67	—	0.0021	NR	1.5	—	1.9
	After coating and calendering	62	46	—	0.00090	NR	1.3	—	1.8
Newsprint	100% TMP	44	60	0.455	0.0095	2.2	1.2	1.9	4.8
	35% RP and 65% TMP	45	57	0.490	0.0089	2.9	1.2	2.0	4.5
	Before calendering	41	85	0.300	0.026	9.9	1.1	1.8	5.5
	After calendering	40	55	0.452	0.011	3.4	1.2	2.0	5.1
Cardboard		238	316	0.468	0.016	7.2	1.1	1.8	2.7
Fine paper		81	105	0.479	0.020	13.5	0.88	1.4	2.4
Pulp sheet	Softwood	882	1540	0.356	0.074	460	0.58	1.93	1.7
	Hardwood	752	1020	0.458	0.039	48	0.58	0.4	1.6
Hand sheets		178	375	0.294	0.115	540	0.60	0.97	1.1
(unbeaten		171	309	0.343	0.079	300	0.53	0.85	1.1
sulphate pulp		172	281	0.379	0.070	190	0.57	0.92	1.1
from softwood		167	237	0.438	0.049	99	0.59	0.95	1.1

NR = not reproducible.

oriented in the least frequently occurring direction. The measurements were performed on a TSO-tester from Lorentzen and Wettre (Sandström and Titus 1995).

5. ASSUMPTIONS ABOUT THE FIBRE STRUCTURE

In the previous studies of gas diffusion through sheets of pulp and paper (Nilsson and Stenström 1995a, b), certain assumptions were made about the structure of the material and the fibres of which the material is composed. In order to compare the results for gas diffusion with those for gas flow, the same assumptions must of course be made here as there. These are outlined below.

From the measurements of basis weight (G) and paper thickness (z), the volume fraction of fibres (ϕ_{tot}) was calculated as

$$\phi_{tot} = \frac{G}{z\rho_{fibre}} \qquad [22]$$

where the density of the cellulose fibres was taken to be $\rho_{fibre} = 1610\ kg/m^3$ (Campbell 1947). This calculation of ϕ_{tot} was not performed for the coated LWC-sheets (see table 2), since the density of the particles in the coating layer is different from that of cellulose.

Even in dried pulp and paper sheets, the collapsed fibres are somewhat hollow. This aspect of porosity has been shown to be attainable for gases and liquids through their penetration of the cell wall pits (Bristow 1986). Although those surfaces are probably included in the specific surface areas measured, transport inside the lumen hardly contributes to any significant degree to the flow process as measured. Thus, a new volume fraction ϕ_e has been defined, representing the sum of the volume fraction of fibres and the volume fraction of lumen, $\epsilon = 1 - \phi_e$ being the porosity where the observed gas flow through the sheet presumably takes place. From measurements made on published SEM pictures of paper cross sections, it was estimated that $\phi_e/\phi_{tot} = 1.2$. The shape of the cellulose fibre suggested in the present study is shown in figure 10.

In order to compare measured and calculated permeabilities it is necessary to also have an estimate of the size of the cellulose fibres, since the fibre hydraulic diameter is input necessary for the theoretical models. In the following, two different methods to estimate the hydraulic diameter of the cellulose fibre are described.

The average length density of kraft pulp fibres of Douglas fir has been measured by Hatton and Cook (1992) as $\rho_{l,fibre} = 2.18 \times 10^{-7}\ kg/m$. If one assumes a cylindrical fibre shape, the hydraulic diameter is that given in [23] below, and if one assumes a band-shaped fibre cross-section the hydraulic diameter for different fibre aspect ratios α is that given below in [24].

$$D_h = 2 \cdot \sqrt{\frac{\rho_{l,fibre} \cdot \phi_e/\phi_{tot}}{\pi \cdot \rho_{fibre}}} \approx 14.38\ \mu m \qquad [23]$$

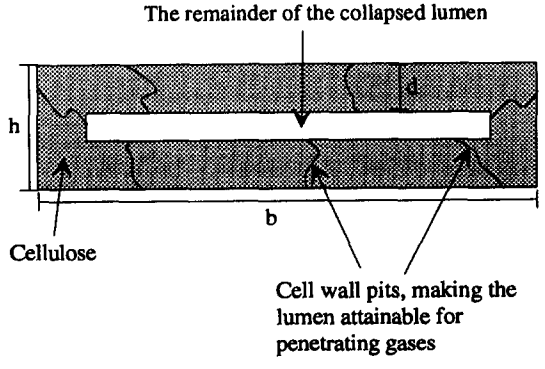

Figure 10. Cross-section of a collapsed cellulose fibre as modelled in the present study.

$$D_h = \frac{4 \cdot \alpha h \cdot h}{2(\alpha h + h)} = 2\frac{\alpha}{\alpha + 1} h = 2\frac{\alpha}{\alpha + 1}\sqrt{\frac{\rho_{l,\text{fibre}}\phi_e/\phi_{tot}}{\rho_{\text{fibre}}\alpha}} \approx \frac{\sqrt{\alpha}}{\alpha + 1} 2.549 \times 10^{-5}\,\text{m}. \quad [24]$$

The other method to estimate the average fibre hydraulic diameter involves combining the specific surface areas measured with the proposed structure of the collapsed cellulose fibre as shown in figure 10. The quotient of the volume fraction of fibres hindering transport (ϕ_e) to the total volume fraction of fibres (ϕ_{tot}) can be expressed as a function of fibre height (h), fibre width (b) and fibre wall thickness (d), as indicated in [25] (see also figure 10). Assuming that both the outer fibre surfaces and the surfaces of the lumen are available for adsorption/desorption of nitrogen molecules during measurement of the specific surface area, the specific surface area of the fibre is that given below in [26].

$$\frac{\phi_e}{\phi_{tot}} = \frac{bh}{bh - (b - 2d)(h - 2d)} = 1.20 \quad [25]$$

$$\tilde{A}_s = \frac{2(b + h + (b - 2d) + (h - 2d))}{bh - (b - 2d)(h - 2d)}. \quad [26]$$

Through taking into account the definition of the fibre aspect ratio $\alpha = b/h$ in combination with the information contained in [25] and [26], the fibre hydraulic diameter can then be calculated from [27] as a function of the fibre aspect ratio α and of the measured specific surface area $\tilde{A}_s$.

$$D_h = \frac{4.8 + 2\sqrt{5.76 - 19.2\alpha/(\alpha + 1)^2}}{\tilde{A}_s}. \quad [27]$$

In figure 11 the hydraulic diameters calculated from [24] are compared with those calculated from [27]. For the specific surface areas as measured for the hand sheets, agreement between the

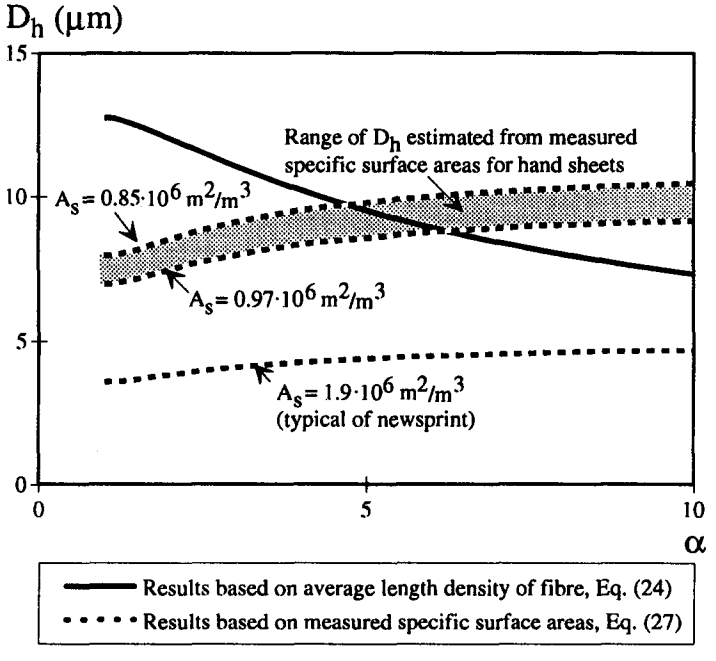

Figure 11. The hydraulic diameter of the cellulose fibre as calculated from the average length density [24] or from the specific surface areas measured [27].

hydraulic diameters calculated in those two ways is quite good, especially so for fibre shapes of $\alpha = 4$–7. It seems therefore that a relatively accurate estimation of the fibre hydraulic diameter for these sheets has been obtained. When one instead inserts into [27] a value of the specific surface area typical of newsprint, the hydraulic diameter becomes much lower. The newsprint sheets probably contain a broad distribution of particles of different sizes, making the assumption of uniform fibre size considerably in error. In the worst case the two estimates of the fibre hydraulic diameter differ by a factor of roughly two.

Of the two methods, the estimation based on the measured average length density was preferred, partly because measurement of that property is more established than measurement of specific surface area by the BET-method and partly because the higher specific surface areas found for newsprint are caused by the presence of fine particles. Such a fine fraction was never included in the structural models upon which the calculated permeabilities are based.

6. RESULTS

6.1. Comparison with experimental data

In figure 12 the measured permeabilities for hand sheets, pulp sheets and newsprint sheets are compared with calculated permeabilities for well-ordered arrangements of cylindrical and

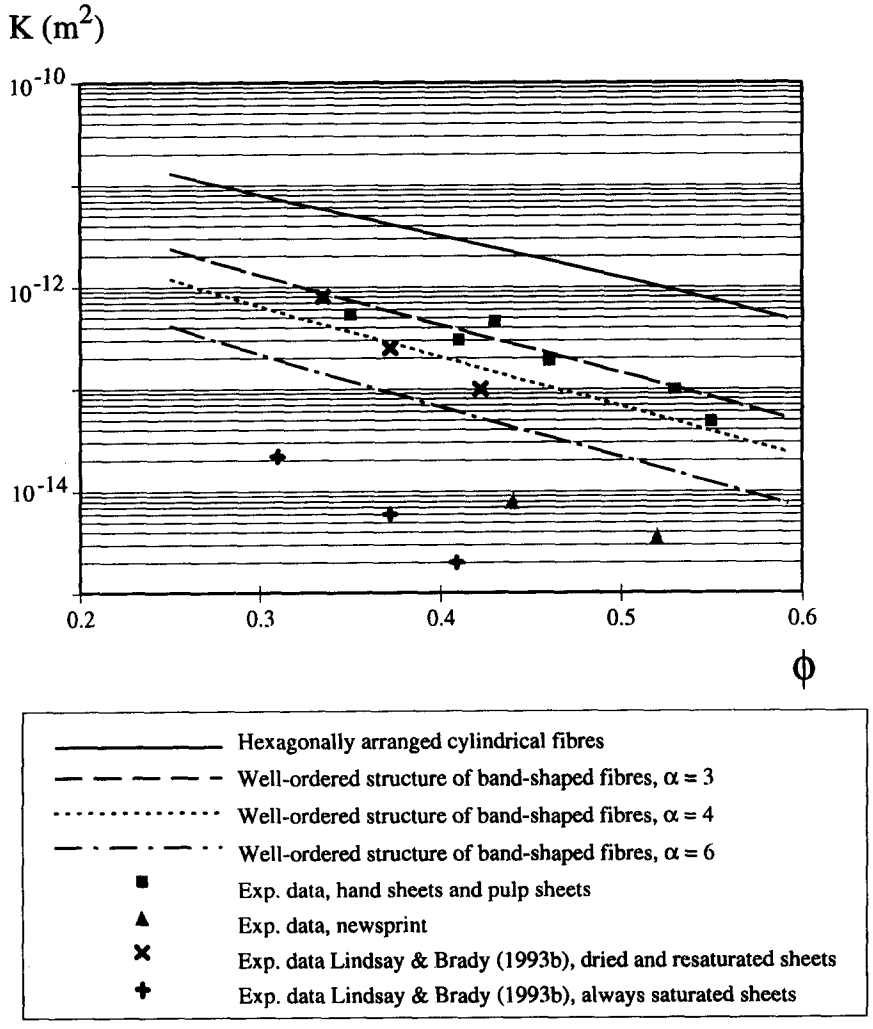

Figure 12. Comparison of measured and calculated permeabilities. The calculated permeabilities were obtained assuming well-ordered structures of cylindrical or band-shaped fibres.

band-shaped fibres, the hydraulic diameters for the cellulose fibres being obtained from [23] and [24], respectively. It is obvious from the results in Table 2 that the permeability is not a function of the volume fraction of fibres alone. Evidently, the measured permeabilities for the hand sheets and the pulp sheets are well described by the assumption of a band-shaped fibre with an aspect ratio of between 3 and 4, which is a physically realistic value. For newsprint sheets the model is obviously not valid, the permeation through these being much slower than the model predicts if physically realistic values for the aspect ratio are taken.

One further conclusion to be drawn from the data in figure 12 concerns structural changes in the cellulose fibres during drying. The data from Lindsay and Brady (1993a, b) are for hand sheets from an unbleached softwood pulp. For those sheets, which were dried at 108°C and resaturated, the measured permeabilities are in agreement with the calculated values (and also with our experimental values for hand sheets and pulp sheets) if a physically realistic value for the aspect ratio ($\alpha \approx 4$) is taken. Those sheets from the same furnish which were always kept saturated, on the other hand, have permeabilities much lower than would be expected on the basis of the model. The increase in permeability caused by the drying of the fibres is attributed by Lindsay and Brady (1993a, b) to a permanent reduction in the swelling capacity of the fibre. Obviously, the structural model proposed here is not relevant for newly formed, wet sheets of paper consisting of swollen cellulose fibres.

Introducing a random fibre distribution causes a sharp increase in permeability as the data in table 1 indicate. On the assumption of a random fibre arrangement the experimental data for hand sheets and pulp sheets are in relatively good agreement with the calculated for $\alpha = 5$. This leads one to compare the aspect ratios used for describing the permeability with those used for describing the effective diffusivity of the hand sheets and the pulp sheets. This comparison is shown in table 3. Regardless of the details of the description of the structure, somewhat higher values of the aspect ratio are needed for describing diffusion than for describing permeation.

The reasons for this discrepancy between the aspect ratios for diffusion and for permeation could be sought within the model itself or in connection with the experimental data. The assumptions made in the model concerning fibre shape, fibre orientation and fibre size might well be less than adequate, which could influence the calculated diffusivities and permeabilities in ways distorting the results. Other deficiencies within the model could be those of incorrect assumptions made concerning the transport mechanisms involved, since in neither case was transport along fibre surfaces or inside the fibres taken into account. Instead the processes were modelled in both cases as taking place within the pores between the fibres. For the air flow process studied here, that assumption is hardly a dubious one, whereas for water vapour diffusion certain data reported in the literature earlier suggest diffusion along fibre surfaces or inside fibres to be of considerable importance (Ahlen 1970). However, it should be pointed out that no observations were made in the experimental study (Nilsson *et al.* 1993) contradicting the hypothesis that the diffusion process took place by ordinary gas diffusion in the pores of the material. Regarding the experimental data, the measurements of paper thickness and permeability all involve standard methods which have been used for many years. Measurements of effective water vapour diffusivity, on the other hand, were made using equipment specially constructed for that purpose. Since equipment of that type has not been used extensively, comparison of the effective diffusivities measured in the present study with data reported in the literature has not been possible.

Table 3. Values of the aspect ratio α employed in describing gas diffusion and gas flow through hand sheets and pulp sheets

Description of paper structure	Type of solution	Gas diffusion	Gas flow
Well ordered fibre arrangement	Analytical solutions	$\alpha \approx 5$	—
Well ordered fibre arrangement	Numerical solutions	$\alpha \approx 5.5$	$\alpha \approx 3.5$
Free-surface models	Numerical solutions	—	$\alpha \approx 3.5$
Random fibre arrangement	Numerical solutions	$\alpha \approx 6$	$\alpha \approx 5$

6.2. Non-dimensional analysis of the experimental data

With a sufficiently accurate description of the structure of the various paper grades and sufficiently accurate knowledge concerning what transport mechanisms are important, each of the properties listed in table 1 could be calculated from the structural work. Since such detailed knowledge is not available it is of interest to also investigate whether these measured properties correlate with each other. Often, when modelling transport in porous media, the structure of the material is described as a bundle of tortuous conduits connecting the two opposing faces of the material. If the assumpiton is made of the conduits having equal size, length and shape, the permeability and the quotient of the effective diffusivity (D_e) of the material to the gas diffusivity (D_G) are given by the expressions in [3] and [28] below

$$\frac{D_e}{D_G} = \frac{1 - \phi_{tot}}{\tau^2}. \qquad [28]$$

The influence of the conduit shape is taken into account by the shape factor k_0, which is 2.0 for a circular pore cross-section and 3.0 for a rectangular slit. The tortuosity can be calculated either from diffusivity measurements ($\tau_{diffusion}$) or from permeability measurements (τ_{flow}). When obtaining the tortuosity from the permeabilty measurements, it was assumed further that the pores have a cylindrical cross-section ($k_0 = 2.0$).

Tortuosities calculated from the diffusivity measurements, together with tortuosities calculated from the permeability measurements are shown in figure 13. There is cleary a correlation between the tortuosities calculated in these two ways. In view of the limiting assumptions made concerning the structure, the tortuosities could hardly have been expected to be equal.

There is no readily available standard method for measuring D_e/D_G such as those used here to measure K and $\tilde{A}_s$. The best non-dimensional correlation relating D_e/D_G to K and $\tilde{A}_s$ is given below in [29]. The correlation between the values of D_e/D_G as calculated from [29] and the measured values is shown in figure 14. The average difference between the calculated and measured values of D_e/D_G is 20%

$$\frac{D_e}{D_G} = 0.02951\phi^{-1.1016}(1 - \phi)^{-0.7982}(K\tilde{A}_s^2)^{0.4936}. \qquad [29]$$

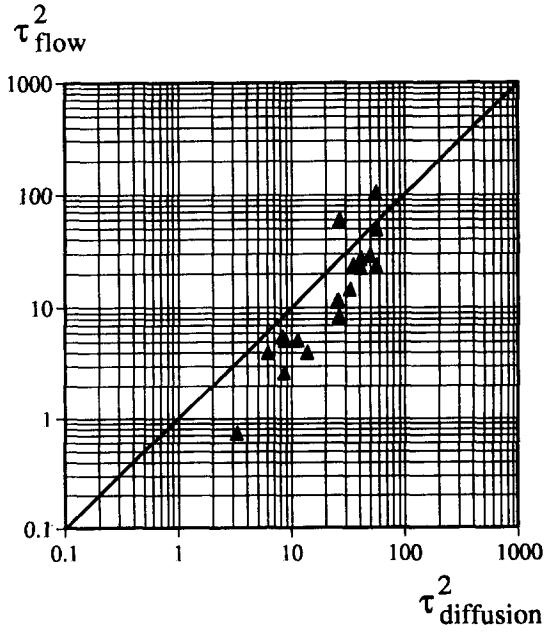

Figure 13. Values of τ^2 calculated from diffusivity measurements and values of τ^2 calculated from permeability measurements.

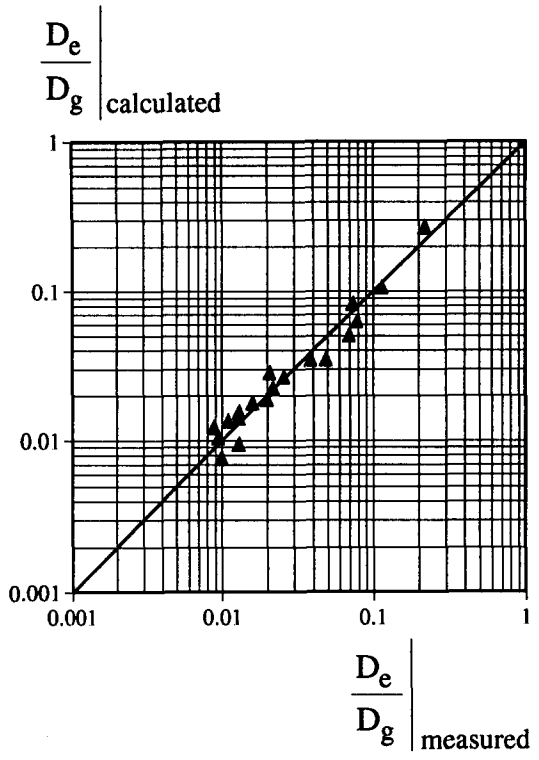

Figure 14. Values of D_e/D_G calculated from the fitted correlation [29] together with the experimental data.

In the present study two-dimensional structural models are used for describing paper structure. Such models could be more severely in error for machine-made paper than for hand sheets and pulp sheets, since in the machine-made paper grades most of the fibres are aligned in the machine direction (see table 2). In table 4 data is given for two commercial grades having almost equal values of volume fraction of fibres and specific surface area, but differing in the degree of fibre orientation. The liner sheet, which has a higher degree of fibre orientation, has a permeability 82% lower than the pulp sheet.

The effects of fibre orientation on permeability were investigated further by forming two hand sheets from unbeaten softwood sulphate pulp. One hand sheet was formed in a static sheet forming equipment resulting in a sheet with a random fibre orientation in the plane of the sheet, and the other was formed in a dynamic sheet forming equipment which gives an oriented sheet similar to a sheet formed in paper machine. By regulating the pressure applied to the hand sheets, equal values of the volume fraction of fibres was obtained for both sheets, $\phi_{tot} = 0.39$. The results show that the permeability of the oriented sheet is 22% lower than that of the sheet without a preferential fibre direction. It thus seems that the low values of permeability and effective diffusivity measured for the machine-made sheets cannot be explained on the basis of fibre orientation alone.

Also, Orloff (1994) measured the Darcian permeability of hand sheets having constant value of volume fraction of fibres, $\phi_{tot} = 0.52$, but which were formed at different ratios of jet to wire

Table 4. Effects of differences in fibre orientation on the permeability. Results for two different commercial grades together with results for handsheets prepared from the same pulp and dried in the same way differing only in the fibre orientation ratio

Paper grade	ϕ_{tot}	$\tilde{A}_s(m^{-1})$	$\frac{TSI_{max}}{TSI_{min}}$	$K(m^2)$
Pulp sheet from hardwood	0.458	1.4×10^6	1.6	4.8×10^{-14}
Liner sheet	0.457	1.4×10^6	2.4	8.5×10^{-15}
Hand sheet with randomly distributed fibres	0.389		1.1	1.8×10^{-13}
Hand sheet with aligned fibres	0.388		2.5	1.4×10^{-13}

velocity. (The larger the difference between the jet velocity and the wire velocity, the more fibres will be oriented in the machine direction.) The jet velocity was kept constant at 316 m/min, and the wire velocity was varied from 800 to 900 m/min. With increasing wire velocity and thereby increasing fibre orientation a slight decrease in permeability could be noticed.

7. CONCLUSIONS

Gas permeation through certain paper grades, such as handsheets of unbeaten pulp and pulp sheets, is well described by a model for flow around band-shaped fibres. Values of the fibre aspect ratio which provide a good fit between experimental data and calculated permeabilities are 3.5 if the structure is assumed to be highly ordered and approximately 5 if a random distribution of the fibres is assumed. These values of the fibre aspect ratio compare favourably with those values used in previous studies of ours (Nilsson and Stenström 1995 a, b) aimed at modelling gas diffusion through these same sheets. Values of the aspect ratio similar to those used for modelling gas permeation through handsheets and pulp sheets can be used when modelling the liquid permeability of dried and resaturated handsheets that has been reported in the literature (Lindsay and Brady 1993a, b), although the permeability is 100 times lower when the sheets are freshly formed from virgin pulp. For other paper grades than those mentioned here, the model is not adequate. Gas permeation through these latter qualities is much slower than that predicted by the model, if physically realistic values for the fibre aspect ratio are taken. For all the paper grades studied here, it was found that the measured permeabilities, effective diffusivities and specific surface areas correlate with each other.

Judging from the experimental results in table 4 it seems unlikely that such low values of permeability as were measured for the machine-made samples could be due to the effects of fibre orientation alone. Another explanation could be the formation of a dense skin in the press section, since it has been shown, assuming two different models of the porous structure, that the presence of serial-type pore nonuniformities leads to a reduction in effective diffusivity and permeability as compared to uniform structures having the same total porosity and total specific surface area (Nilsson and Stenström 1996b). However, in order to include such nonuniformities in the structural models, thickness profiles of porosity and particle sizes need to be measured.

The mechanical pulps used for the production of newsprint contain a larger amount of short fibres, fine fractions and fibre fragments than chemical pulp. To increase the printing quality of newsprint filler material is added. The effects of the presence of such particles on the permeability is difficult to estimate, since it seems that information about the shape, size and orientation of those particles is not readily available in the literature.

Work is needed in modelling other transport processes through sheets of pulp and paper describing the structure of the paper material in the same way as here. Among such transport processes are those of the liquid absorption into dry sheets and of the capillary redistribution of liquid water from larger to smaller pores during the drying process. Since transport within the fibre wall is not taken into account in the present structural model of the paper sheet, account only being taken of transport within the pore space between the fibres, the present models could be assumed to be better suited to modelling the drying of paper from recycled pulp than the drying of paper from virgin pulp. In drying of the latter type transport of water within the fibre wall and structural changes in the fibres during drying would well be important.

Acknowledgements—We wish to thank Anette Lindé and Hilding Ekman from STFI, Stockholm, for performing the measurements of permeability and fibre orientation, and Birgitta Svensson from the Department of Chemical Engineering II for the sound advice she gave us on use of the BET-method.

REFERENCES

Ahlen, A. T. (1970) Diffusion of sorbed water vapor through paper and cellulose film. *Tappi* **53,** 1320–1326.

Bliesner, W. C. (1964) A study of the porous structure of fibrous sheets using permeability techniques. *Tappi* **47,** 392–400.

Bristow, J. A. (1986) The pore structure and the sorption of liquids. In *Paper—Structure and Properties*, eds J. A. Bristow and P. Kolseth, pp. 183–201. Marcel Dekker, New York.

Brown, G. R. (1975) Creeping flow of fluids through assemblages of elliptic cylinders and its application to the permeability of fiber mats. Ph.D. thesis, The Institute of Paper Chemistry, Appleton, Wisconsin.

Brunauer, S., Emmett, P. H. and Teller, E. (1938) Adsorption of gases in multimolecular layers. *J. Am. Chem. Soc.* **60,** 309–319.

Campbell, W. B. (1947) The physics of water removal. *Pulp Paper Mag. Can.* **48,** 103–110.

Carman, P. C. (1937) Fluid flow through granular beds. *Trans. Inst. Chem. Eng. London* **15,** 150–166.

Couture, F., Jomaa, W. and Puiggali, J.-R. (1994) Drying behaviour as influenced by the relative permeability relations. In *Drying '94*, eds V. Rudolph and R. B. Keey, pp. 263–276.

Drummond, J. E. and Tahir, M. I. (1984) Laminar viscous flow through regular arrays of parallel solid cylinders. *Int. J. Multiphase Flow* **10,** 515–540.

Epstein, N. and Masliyah, J. H. (1972) Creeping flow through clusters of spheroids and elliptical cylinders. *Chem. Eng. J.* **3,** 169–175.

Fellers, C., Andersson, H. and Hollmark, H. (1986) The definition and measurement of thickness and density. In *Paper—Structure and Properties*, eds J. A. Bristow and P. Kolseth, pp. 151–167. Marcel Dekker, New York.

FIDAP 7.0 (1993) FIDAP reference manuals. published by Fluid Dynamics International, Inc.

Göttsching, L. and Rhodius, L. (1978) Der Trocknungsverlauf von Papier und Pappe in Abhängigkeit von trocknungstechnischen und papiertechnologischen Parametern. *Das Papier* **32,** 49–58.

Happel, J. (1959) Viscous flow relative to arrays of cylinders. *AIChE J.* **5,** 174–177.

Hatton, J. V. and Cook, J. (1992) Kraft pulps from second-growth Douglas fir: relationships between wood fiber, pulp and handsheet properties. *Tappi J.* **75,** 137–144.

Jackson, G. W. and James, D. F. (1986) The permeability of fibrous porous media. *Can. J. Chem. Eng.* **64,** 364–374.

Jönsson, K. A.-S. and Jönsson, B. T. L. (1992a) Fluid flow in compressible porous media. I: Steady-state conditions. *AIChE J.* **38,** 1340–1348.

Jönsson, K. A.-S. and Jönsson, B. T. L. (1992b) Fluid flow in compressible porous media: II: dynamic behaviour. *AIChE J.* **38,** 1349–1356.

Kozeny, J. (1927) Über kapillare Leitung des Wassers im Boden (Aufstieg, Versickerung und Anwendung auf die Bewässerung). *Sitzber. Akad. Wiss. Wien, Math. Naturw. Klasse* **136,** 271–305.

Labrecque, R. P. (1968) The effects of fibre cross-sectional shape on the resistance to the flow of fluids through fibre mats. *Tappi* **51,** 8–15.

Lindsay, J. D. and Brady, P. H. (1993a) Studies of anisotropic permeability with applications to water removal in fibrous webs. Part 1—Experimental methods, sheet anisotropy, and relationships to freeness. *Tappi J.* **76,** 119–127.

Lindsay, J. D. and Brady, P. H. (1993b) Studies of anisotropic permeability with applications to water removal in fibrous webs. Part 2—Water removal and other factors affecting permeability. *Tappi J.* **76,** 167–174.

Lindström, T. and Söderberg, G. (1986) On the mechanism of sizing with alkylketene dimers. Part 1. Studies on the amount of alkylketene dimer required for sizing different pulps. *Nordic Pulp Paper Res. J.* **1,** 26–33, 42.

Mohlin, U.-B. and Gray, D. G. (1974) Gas chromatography on polymer surfaces: adsorption on cellulose. *J. Coll. Int. Sci.* **47,** 747–754.

Nilsson, L., Wilhelmsson, B. and Stenström, S. (1993) The diffusion of water vapour through pulp and paper. *Drying Techn.* **11,** 1205–1225.

Nilsson, L. and Stenström, S. (1995a) Gas diffusion through sheets of fibrous porous media. *Chem. Eng. Sci.* **50,** 361–371.

Nilsson, L. and Stenström, S. (1995b) Modelling the effective mass and heat diffusivities of pulp and uncoated paper. *Proceedings of ASME HTD*, Vol. 317-2, pp. 421–426.

Nilsson, L., Månsson, S. and Stenström, S. (1996a) Measuring moisture gradients in cellulose fibre networks: an application of the magnetic resonance imaging method. *J. Pulp Paper Sci.* **22,** J48–J52.

Nilsson, L. and Stenström, S. (1996b) Effects of serial and parallel pore nonuniformities: results from two models of the porous structure. *Transp. Porous Media* (to appear).

Orloff, D. I. (1994) Impulse drying of recycled multi-ply linerboard: laboratory-scale studies. *Tappi J.* **77,** 169–179.

Persson, H. (1994) A literature review of impulse drying 1988–1994. Department of Chemical Engineering I. LUTKDH/(TKKA-7005)/1-42/(1994). Lund University, Sweden.

Sampson, W. W. and Bridle, I. J. (1995) Simulation of the directional dependence of flow through fiber mats. *Nordic Pulp Paper Res. J.* **10,** 145–147, 149.

Sandström, J. and Titus, M. (1995) Field experience in prediction of corrugated board strength with ultrasonic testing. *Tappi J.* **78,** 240-19–240-22.

Sangani, A. S. and Acrivos, A. (1982) Slow flow past periodic arrays of cylinders with application to heat transfer. *Int. J. Multiphase Flow* **8,** 193–206.

Schlünder, E.-U. (1988) On the mechanism of the constant drying rate period and its relevance to diffusion controlled catalytic gas phase reactions. *Chem. Eng. Sci.* **43,** 2685–2688.

Wang, C. Y. (1996) Stokes flow through an array of rectangular fibers. *Int. J. Multiphase Flow* **22,** 185–194.

APPENDIX

Verification of the Assumption of Creeping Flow

The validity of Darcy's law was tested by performing peremeability measurements on different number of paper sheets (n). These tests were performed for the handsheets for which $\phi_{tot} = 0.438$. Since the average flow velocity is equal to the volume (V) divided by the time required for penetration (t) and the available sample area (A_{sample}), one finds upon rearrangement of Darcy's

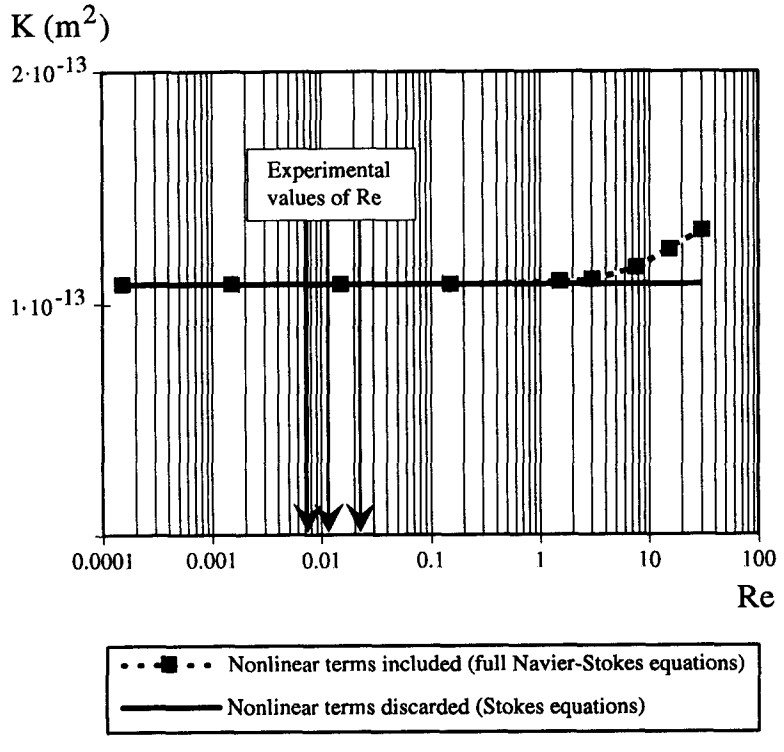

Figure A1. Theoretically calculated limit of the Reynolds number for the creeping flow assumption to apply together with the estimates of the Reynolds number obtained in the experiments.

law [1] that the time recorded should be proportional to the number of sheets. Indeed, this is also the relationship found experimentally. The validity of Darcy's law that is demonstrated there serves to support the assumption of creeping flow behaviour occurring in the pores.

Further tests involved comparing for the free-surface model the solution of the full Navier–Stokes equation [5] with that of the Stokes equation [6], assuming there to be a fibre aspect ratio of $\alpha = 3.2$. The calculations were performed for a structure in which $\phi_{tot} = 0.438$, corresponding to the porosity of the hand sheets used for testing behaviour pertaining to Darcy's law. Assuming $\alpha = 3.2$, the hydraulic fibre diameter was calculated from [24] to be $D_h = 10.9\ \mu m$. The permeabilities calculated are shown for different values of the Reynolds number in figure A1, the Reynolds number being defined as

$$\mathrm{Re} = \frac{vD_h\rho}{\mu}. \qquad [30]$$

The Reynolds numbers obtained in the experiments were 0.021, 0.0108 and 0.0072 for the three cases. Judging from the results presented in figure A1, the experiments are within the range of the Reynolds numbers for which the creeping flow assumption is valid.